

**$^{77}\text{Se}$  NMR investigation of the field-induced spin-density-wave transitions in  $(\text{TMTSF})_2\text{ClO}_4$** L. L. Lumata,<sup>1</sup> J. S. Brooks,<sup>1</sup> P. L. Kuhns,<sup>1</sup> A. P. Reyes,<sup>1</sup> S. E. Brown,<sup>2</sup> H. B. Cui,<sup>1</sup> and R. C. Haddon<sup>3</sup><sup>1</sup>*Department of Physics and National High Magnetic Field Laboratory, Florida State University, Tallahassee, Florida 32310, USA*<sup>2</sup>*Department of Physics and Astronomy, University of California at Los Angeles, Los Angeles, California 90095, USA*<sup>3</sup>*Department of Chemical and Environmental Engineering, University of California, Riverside, California 92521, USA*

(Received 28 May 2008; published 25 July 2008)

Complementary  $^{77}\text{Se}$  nuclear magnetic resonance (NMR) and electrical transport have been used to correlate the spin-density dynamics with the subphases of the field-induced spin-density wave (FISDW) ground state in  $(\text{TMTSF})_2\text{ClO}_4$ . We have found that the peaks in the spin-lattice relaxation rate  $1/T_1$  appear within the metal-FISDW phase boundary and/or at first-order subphase transitions. In the quantum limit above 25 T, the NMR data have given an insight into the FISDW electronic structure.

DOI: 10.1103/PhysRevB.78.020407

PACS number(s): 75.30.Gw, 74.70.Kn, 76.60.-k

The effects of high magnetic fields on the quasi-one- and two-dimensional electronic structure of organic conductors is a rich area of investigation.<sup>1</sup> In Bechgaard and related salts,<sup>2,3</sup> which remain metallic at low temperatures, a magnetic field applied parallel to the least conducting direction (perpendicular to the conducting chains) produces a field-induced spin-density wave (FISDW) ground state.<sup>4</sup> A simple description of this effect is that the magnetic field decreases the amplitude of the lateral motion of the carriers as they move along the conducting chains; thereby, making the electronic structure increasingly more one dimensional (1D). Hence, eventually, 1D instabilities become favorable. In reference to Fig. 1, a nested quasi-1D Fermi surface (FS) is induced at a second-order phase boundary, where a FISDW gap opens above a threshold field  $B_{\text{th}}$  (Ref. 5). Due to quantization of the nesting vector  $Q=(2k_F \pm N2\pi/\lambda, \pi/b)$  (where  $\lambda=h/ebB$ ), increasing magnetic field produces a first-order “cascade” of FISDW subphases. In the quantum limit, the optimum nesting vector (where  $N=0$ ) yields the final FISDW state in the case of  $(\text{TMTSF})_2\text{PF}_6$ , which has a single quasi-one-dimensional Fermi surface (Q1D FS) (Ref. 6).

However,  $(\text{TMTSF})_2\text{ClO}_4$  experiments show additional phase boundaries in the quantum limit.<sup>7-11</sup> Since the ordering of the tetrahedral  $\text{ClO}_4$  anions below 24 K doubles the unit cell along the interchain direction  $b'$ , zone folding produces two Q1D FS sheets, leading to complex high-field behavior.<sup>9,10</sup> Recently, a model<sup>12</sup> has been proposed, where both FS sheets are gapped at the Fermi level  $E_F$  in the FISDW region; but above the “reentrant” phase boundary  $B_{\text{re}}$  (Ref. 8), only one of the sheets is gapped at  $E_F$ . This leads to an explanation for the oscillatory sign reversal of the Hall effect<sup>13</sup> above  $B_{\text{re}}$ .

In this Rapid Communication, we present complementary measurements of electrical transport and pulsed  $^{77}\text{Se}$  ( $\gamma=8.13$  MHz/T) NMR in  $(\text{TMTSF})_2\text{ClO}_4$ ; both for variable frequency and magnetic field, and by rotating the sample in the  $b'-c^*$  plane at constant frequency and magnetic field [see inset of Fig. 3(c) for definitions of crystal axes and field direction  $\theta$ ]. The orbital nature of the FISDW transitions<sup>14</sup> allows a continuous sweep of the perpendicular field  $B_{\perp}=B \cos(\theta)$  from 0 T for  $B\parallel b'$  to 30 T (in the present case) for  $B\parallel c^*$ , thereby accessing the entire metallic and FISDW field range by sample rotation at constant NMR frequency.

A single crystal of  $(\text{TMTSF})_2\text{ClO}_4$  was inserted into a miniature NMR coil with the  $a$  axis aligned parallel with the coil axis. Gold wires (12  $\mu\text{m}$ ) were attached with carbon paint for four-terminal  $ac$  resistance measurements with a current of 1  $\mu\text{A}$  applied along the  $c^*$  axis. The sample and coil were mounted on a probe with single-axis goniometer and cooled at a rate of 30 mK/min from 30 to 18 K to allow anion ordering. For variable field measurements, the NMR frequency was changed for each field while for rotation measurements at fixed field  $B_{\text{max}}$  in the  $b'-c^*$  plane, the frequency was fixed at  $\gamma B_{\text{max}}$ .

The spin-density-wave nature of the ground state has been described in the Bechgaard salts by NMR studies.<sup>15,16</sup> The characteristic NMR lineshape in the SDW phase involves multiple peaks due to the antiferromagnetic nature of the local fields, and the peak separations vary systematically with field orientation due to changes in the dipolar coupling with respect to the  $(\text{TMTSF})_2\text{ClO}_4$  donor axes.<sup>17,18</sup>

NMR pulse optimization involved  $\pi/2-\pi/2$  pulse trains to obtain the maximum NMR intensity at the optimum pulse widths  $\tau_M$  in the metallic and  $\tau_{\text{sdw}}$  in the FISDW phases. Typically, in the metallic state, the optimum  $\pi/2$  pulse width was  $\tau_M=1$   $\mu\text{s}$  while in the FISDW region,  $\tau_{\text{sdw}}$  was varied from 50 to 500 ns. Since the same pulse power level (12 W)

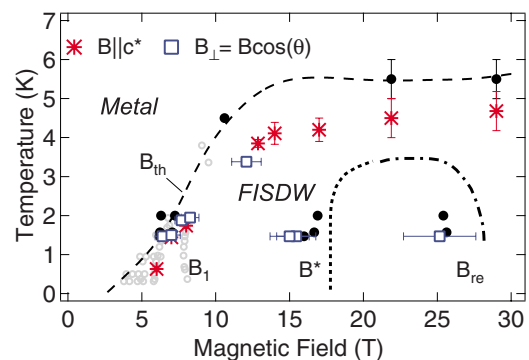


FIG. 1. (Color online) Phase diagram of  $(\text{TMTSF})_2\text{ClO}_4$  for  $B\parallel c^*$  derived from previous reports (Refs. 5, 9, 11, and 19), (dashed lines) including a summary of the observed  $^{77}\text{Se}/T_1$  peaks (asterisks and open squares), and the corresponding features in the transport measurements (dark and gray circles) from this work. (Field labels defined in text.)

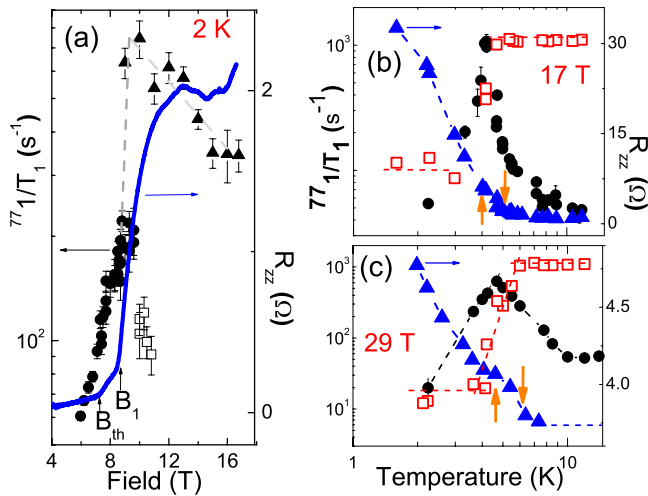


FIG. 2. (Color online) (a) Field-dependent  $1/T_1$  and resistance at 2 K ( $\theta=25^\circ$ ). Solid circles and open squares: metallic pulses; solid triangles: enhanced FISDW pulses; (b) and (c) temperature dependence of  $1/T_1$  (solid circles),  $R_{zz}$  (solid triangles), and the integrated NMR intensity with Boltzmann factor correction (open squares) for  $B\parallel c^*$ . The down arrow indicates the upturn in  $R_{zz}$  and the up arrow indicates the peak  $1/T_1$ .

was used for all measurements, the rf-enhancement factor<sup>19</sup> was obtained from the relation  $\eta \equiv \tau_M / \tau_{sdw}$ . The spin-lattice relaxation rate  $1/T_1$  was defined using a single-exponential form for the magnetization recovery and varied by less than 10% over the spectrum in all cases. In the FISDW, there is a slight deviation (approximately 5% in the initial slope) from the exponential recovery, not uncommon for these systems.<sup>18</sup> Long recycle times (0.5 to 5 s) were used to avoid sample heating.

We first discuss the results at constant angle, where the field (and frequency) were changed to access the different FISDW phases. In Fig. 2(a), the magnetic-field-dependent  $1/T_1$  and the corresponding  $c^*$ -axis resistance ( $R_{zz}$ ) are shown for 2 K. For constant temperature, as the metal-FISDW transition is approached and  $B_{th}$  is crossed,  $1/T_1$  gradually increases. It is not until the predominant first-order subphase transition  $B_1$  is reached that  $1/T_1$  exhibits a maximum. For further increases in field,  $1/T_1$  decreases. The metallic pulses were optimum when  $B < B_1$ ; but at higher fields, the shorter  $\tau_{sdw}$  pulses were necessary to follow the signal into the FISDW phase. In Figs. 2(b) and 2(c), the variation of  $1/T_1$  with temperature is shown, along with  $R_{zz}$  and the Boltzmann-factor-normalized NMR intensity. The temperature dependence of  $1/T_1$  generally follows a critical fluctuation behavior of  $1/T_1 \approx (T - T_{SDW})^{-1/2}$  above the peak and a power-law behavior of  $(1/T_1 \approx T^{1.2})$  at lower temperatures. The spin density is constant in the metallic state and drops exponentially starting in the second-order phase boundary. Simultaneous resistance measurements show the onset of semimetallic behavior at this same temperature. We emphasize here that the peaks in  $1/T_1$  occur at temperatures that are systematically below the second-order phase boundary, as indicated by the resistance anomaly and the signal intensity. The positions of the peaks in  $1/T_1$  and the corresponding phase boundaries from transport measurements are presented in Fig. 1 for all field-dependent data.

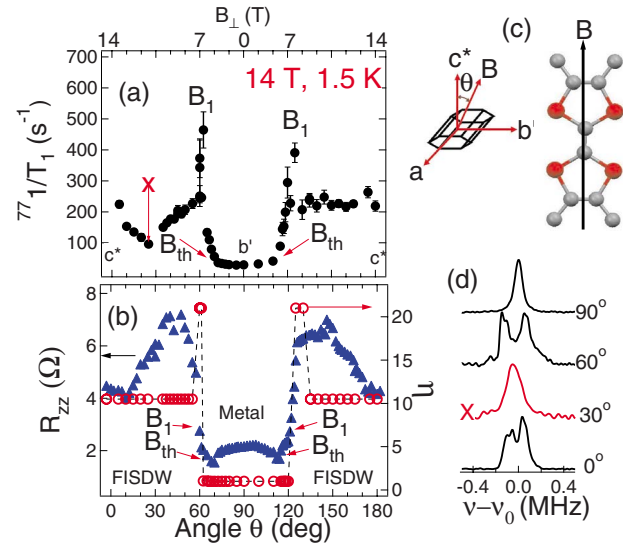


FIG. 3. (Color online) Angular-dependent NMR and electrical transport at 14 T and 1.5 K in  $(TMTSF)_2ClO_4$ . (a)  $1/T_1$  vs field orientation. (b) Corresponding magnetoresistance and enhancement  $\eta$  at 14 T. (c) Schematic of the crystal axes and orientation of the TMTSF molecule at point X where the dip in  $1/T_1$  occurs. (d) Representative spectra at various angles (X represents the spectrum at the dip in  $1/T_1$ ).

The angular-dependent data shown in Fig. 3 at 14 T (118.32 MHz) and 1.5 K provide more details about the second-order  $B_{th}$  and first-order  $B_1$  FISDW transitions. In the angle range of  $70^\circ < \theta < 110^\circ$ , the sample is metallic, which is also shown in magnetoresistance (MR) and  $\eta=1$ . There is a slight increase of (10 s<sup>-1</sup>) in  $1/T_1$  as the field rotates away from the  $b'$  axis in the metallic state. When  $B_\perp$  reaches  $B_{th}=6.25$  T, there is an increase in  $1/T_1$  corresponding to a sharp feature in the resistance. Note however that for  $B_{th} < B_\perp < B_1$ ,  $\eta=1$  as in the metallic phase. In Fig. 2(a), the peak in  $1/T_1$  occurs at  $B_1$  where  $\eta \approx 20$ . Deep in the FISDW phase, the NMR lineshapes broadened and have a double-peaked structure. Since the  $a$  axis used for the rotation data is also the symmetry axis for the hyperfine coupling, anisotropy in  $1/T_1$  is indiscernible in the metallic phase<sup>22</sup> and negligible in the FISDW phase (a few percent) compared to the large variation in  $1/T_1$  at the different phase boundaries. In the angular dependence, there is a special symmetry position at  $\theta \approx 25^\circ$ , where the magnetic field is parallel to the  $x$  axis of the TMTSF donor molecule. Here,  $1/T_1$  exhibits a dip (marked X in Fig. 3); the lineshape narrows to a single peak. This dip feature has been previously reported for  $(TMTSF)_2PF_6$  (Ref. 16) and is not related to the magic-angle (MA) effects<sup>20</sup> reported in  $(TMTSF)_2ClO_4$  (Ref. 21). Although the FISDW data are always above the spin-flop field ( $< 0.5$  T), there is a spin rotation from the  $a$  axis to the  $c^*$  axis when the field direction approaches  $B\parallel c^*$ , which has been associated with the dip phenomena.<sup>16</sup> Likewise, there is no evidence for the MA effects in the NMR signal in accord with previous studies on  $(TMTSF)_2PF_6$  (Ref. 22).

In Fig. 4, the high-field ( $B_{max}=30$  T) angular-dependent NMR results for  $1/T_1$ ,  $B_1$ ,  $B^*$ ,  $B_{re}$ , and  $\eta$  are shown along with the corresponding MR data at  $T=1.47$  K and at 243.9

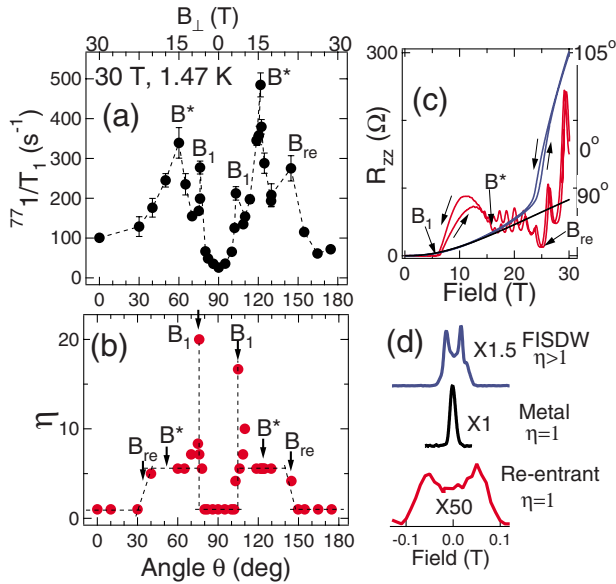


FIG. 4. (Color online) Angular-dependent NMR and electrical transport at  $B=30$  T, 1.47 K. (a) Metallic and FISDW phase transitions revealed in angular-dependent  $1/T_1$ . (b) The enhancement vs  $\theta$ . Of special note is that  $\eta=1$  above  $B_{re}$ . (c) Representative MR at different angles at 1.47 K. For each trace, the NMR measurement was made at 30 T; hence, above  $B_{re}$  for  $\theta=0^\circ$ , above  $B_1$  for  $\theta=105^\circ$ , and in the metallic phase for  $\theta=90^\circ$ . (d) Corresponding fieldswept spectra at  $\nu_0=243.9$  MHz (30 T) at different phases.

MHz. In Fig. 3, the rotation away from the metallic phase at  $B \parallel b'$  (i.e., for increasing  $B_\perp$ ) causes  $1/T_1$  to increase as  $B_{th}$  is entered; but it is not until the first-order boundary  $B_1$  is crossed that  $1/T_1$  reaches a maximum. Since  $B_{max}=30$  T, the full-field range in  $B_\perp$  can be accessed: additional peaks in  $1/T_1$  are observed for  $B_\perp=B^*$  in the range of 15–17 T [which corresponds to a characteristic feature in the MR seen in many experiments (Ref. 9)] and also for  $B_\perp=B_{re}$ . Of specific note is the corresponding behavior of  $\eta$ , which falls from five to one, when the  $B_{re}$  boundary is crossed for both positive and negative field directions. The main changes in spectral linewidth due to the internal field occur at the metal-FISDW transition, not at the subphase transitions. Hence, the enhancement factor and the increase in  $1/T_1$ , and not a significant change in the internal field, characterize the  $B_{re}$  phase boundary. For  $\theta \approx 25^\circ$  in Fig. 4(a), the feature corresponding to  $B_\perp=B_{re}$  is obscured, most likely because it occurs where the dip (see Fig. 2) in  $1/T_1$  appears. The results from Fig. 4 are summarized in Fig. 1.

Most significant in the present work is the location of the peaks in  $1/T_1$  in the different FISDW phases, and the behavior of the NMR signal above the re-entrant phase boundary.

First, for  $1/T_1$  data at constant field, the peaks in  $1/T_1$  appear at temperatures as much as 30% lower than the second-order phase boundary (Fig. 1). Hanson *et al.*<sup>23</sup> have previously suggested that the true signature of the second-order onset of the FISDW occurs at the  $1/T_1$  peak, not at the higher temperature onset of transport anomalies. However, the rapid oscillation (RO) behavior [see, e.g., Fig. 4(c)] is very sensitive to the FS nesting conditions and a transition between Stark interference behavior (metallic) and anoma-

lous RO behavior (FISDW) is coincident with the second-order phase boundary.<sup>9,10,24</sup> The spin density and the onset of semimetallic behavior in  $R_{zz}$  also begins to change at this boundary [Fig. 2(c)] [see also Fig. 6(a) in Ref. 9]. We therefore assert that the FISDW phase boundary, i.e., the second-order line appears when the FS nesting (and gap) first appears; that is, *above* the temperature where the peaks in  $1/T_1$  appear. From Figs. 2(b) and 2(c), this effect occurs approximately at the inflection point of the drop in the spin density (50%). In contrast, we note that in  $(\text{TMTSF})_2\text{PF}_6$ , where under ambient conditions, a SDW transition occurs at 12 K; the resistance shows a sharp increase,<sup>25</sup> which is nearly coincident with a peak in  $1/T_1$  (Ref. 26) with an uncertainty of less than 10%. Hence, there appears to be a difference in the way that the order parameter develops below the SDW and the FISDW phase boundaries. Critical slowing of the fluctuations near a SDW transition ordinarily leads to a peak in relaxation rate at  $T_c$ . Below  $T_c$ , relaxational (dynamical) effects have been observed,<sup>27</sup> which cannot be ruled out. However, a density-of-states effect similar to the Hebel-Slichter peak seen in superconductors<sup>28</sup> is also possible.

Second, in both field dependent and rotation experiments, we find that  $1/T_1$  exhibits peaks within the second-order phase boundary, in particular at the first-order phase lines  $B_1$ ,  $B^*$ , and  $B_{re}$ . Since the first-order transitions involve transitions between the different subphases, domain-wall effects may cause the peaks in  $1/T_1$  as these boundaries are crossed.<sup>29</sup>

Third, in the rotation experiments, the enhancement parameter  $\eta$  was monitored in detail. The effect is associated with rf-induced displacement or depinning of the SDW phase by the electric fields. There is no enhancement ( $\eta=1$ ) in the metallic phase; in the FISDW phase,  $\eta$  will increase according to the ability of the electric field to modulate the condensate.<sup>30</sup> The electric fields associated with depinning are typically 5 mV/cm or less.<sup>31,32</sup> In the present case, we estimate the ac electric field in the NMR coil to be of the order 1 to 10 V/cm (see also previous estimates in Ref. 19), well above the depinning field. Notably, at the transition  $B_{re}$ , the enhancement factor drops to unity; but the NMR spectrum is still double peaked and characteristic of antiferromagnetic structure [Fig. 4(d)]. Based on the recent band model<sup>12</sup> in the reentrant phase, the FISDW will be associated with one of the bands (FS1—giving rise to the SDW spectrum): but the other band (FS2) is metallic at the Fermi level (reducing the effective electric field). Hence, we propose that the electric field in the half-metallic phase above  $B_{re}$  is attenuated, thereby reducing  $\eta$ .

In summary, we have correlated the transport features, which describe the FISDW phase diagram of  $(\text{TMTSF})_2\text{ClO}_4$  with  $^{77}\text{Se}$  NMR. We find that the peaks in  $1/T_1$  occur within (not at) the second-order phase boundary. Furthermore, angular-dependent measurements facilitate the crossing of FISDW subphase boundaries at constant temperature, where peaks in  $1/T_1$  are also observed, indicating changes in the nesting configurations at these transitions. At high fields, the drop in the rf-enhancement parameter upon crossing the re-entrant phase boundary is consistent with the expectation that only one FS sheet is nested above  $B_{re}$ . We expect that this electronic configuration (only one FS sheet may be

nested) is also the case in the broader region between the second-order phase boundary and the underlying first-order phases at lower temperatures.

We thank V. F. Mitrovic for helpful suggestions. This

work was supported in part by NSF Contracts No. DMR-0602859 (J.S.B.) and No. DMR-0520552 (S.E.B.) and performed at the National High Magnetic Field Laboratory, supported by NSF DMR-0084173, by the State of Florida, and by the DOE.

- 
- <sup>1</sup>T. Ishiguro, K. Yamaji, and G. Saito, *Organic Superconductors II* (Springer-Verlag, New York, 1998).
- <sup>2</sup>K. Oshima, H. Okuno, K. Kato, R. Maruyama, R. Kato, A. Kobayashi, and H. Kobayashi, *Synth. Met.* **70**, 861 (1995).
- <sup>3</sup>N. Biskup, J. S. Brooks, R. Kato, and K. Oshima, *Phys. Rev. B* **60**, R15005 (1999).
- <sup>4</sup>P. M. Chaikin, *J. Phys. I* **6**, 1875, (1996).
- <sup>5</sup>F. Pesty, P. Garoche, and K. Bechgaard, *Phys. Rev. Lett.* **55**, 2495 (1985).
- <sup>6</sup>W. Kang, S. T. Hannahs, and P. M. Chaikin, *Phys. Rev. Lett.* **70**, 3091 (1993).
- <sup>7</sup>T. Osada, N. Miura, and G. Saito, *Solid State Commun.* **60**, 441 (1986).
- <sup>8</sup>M. J. Naughton, R. V. Chamberlin, X. Yan, S.-Y. Hsu, L. Y. Chiang, M. Ya. Azbel, and P. M. Chaikin, *Phys. Rev. Lett.* **61**, 621 (1988). As first described in this reference, we refer to the low-temperature phase boundary near 26 T as “re-entrant,” although only one FS sheet returns to a metallic state.
- <sup>9</sup>O.-H. Chung, W. Kang, D. L. Kim, and C. H. Choi, *Phys. Rev. B* **61**, 11649 (2000).
- <sup>10</sup>S. Uji, J. S. Brooks, M. Chaparala, S. Takasaki, J. Yamada, and H. Anzai, *Phys. Rev. B* **55**, 14387 (1997).
- <sup>11</sup>S. K. McKernan, S. T. Hannahs, U. M. Scheven, G. M. Danner, and P. M. Chaikin, *Phys. Rev. Lett.* **75**, 1630 (1995).
- <sup>12</sup>S. K. McKernan, S. Uji, J. S. Brooks, and P. M. Chaikin, *Solid State Commun.* **145**, 385 (2008).
- <sup>13</sup>S. Uji, S. Yasuzuka, T. Konoike, K. Enomoto, J. Yamada, E. S. Choi, D. Graf, and J. S. Brooks, *Phys. Rev. Lett.* **94**, 077206 (2005).
- <sup>14</sup>G. S. Boebinger, G. Montambaux, M. L. Kaplan, R. C. Haddon, S. V. Chichester, and L. Y. Chiang, *Phys. Rev. Lett.* **64**, 591 (1990).
- <sup>15</sup>J. M. Delrieu, M. Roger, Z. Toffano, A. Moradpour, and K. Bechgaard, *J. Phys. (Paris)* **47**, 839 (1986).
- <sup>16</sup>T. Takahashi, Y. Maniva, H. Kawamura, and G. Saito, *J. Phys. Soc. Jpn.* **55**, 1364 (1986).
- <sup>17</sup>M. Takigawa and G. Saito, *J. Phys. Soc. Jpn.* **55**, 1233 (1986).
- <sup>18</sup>F. Zhang, Y. Kurosaki, J. Shinagawa, B. Alavi, and S. E. Brown, *Phys. Rev. B* **72**, 060501(R) (2005).
- <sup>19</sup>M. Takigawa and G. Saito, *Physica B (Amsterdam)* **143**, 422 (1986).
- <sup>20</sup>A. G. Lebed and P. Bak, *Phys. Rev. Lett.* **63**, 1315 (1989).
- <sup>21</sup>M. J. Naughton, O. H. Chung, M. Chaparala, X. Bu, and P. Coppens, *Phys. Rev. Lett.* **67**, 3712 (1991).
- <sup>22</sup>W. Wu, P. M. Chaikin, W. Kang, J. Shinagawa, W. Yu, and S. E. Brown, *Phys. Rev. Lett.* **94**, 097004 (2005).
- <sup>23</sup>M. E. Hanson, M. Horvatic, C. Berthier, Y. Fagot-Reverat, D. Jerome, and C. Bourbonnais, *Bull. Am. Phys. Soc.* **43**, 130.12 (1998).
- <sup>24</sup>S. Uji, J. S. Brooks, M. Chaparala, S. Takasaki, J. Yamada, and H. Anzai, *Phys. Rev. B* **55**, 12446 (1997).
- <sup>25</sup>K. Bechgaard, C. S. Jacobson, K. Mortensen, H. J. Pedersen, and N. Thorup, *Solid State Commun.* **33**, 1119 (1980).
- <sup>26</sup>S. Valfells, P. Kuhns, A. Kleinhammes, J. S. Brooks, W. Moulton, S. Takasaki, J. Yamada, and H. Anzai, *Phys. Rev. B* **56**, 2585 (1997).
- <sup>27</sup>W. G. Clark, M. E. Hanson, W. H. Wong, and B. Alavi, *J. Phys. IV* **3**, C2-235 (1993).
- <sup>28</sup>D. E. MacLaughlin, in *Solid State Physics*, edited by H. Ehrenreich, F. Seitz, and D. Turnbull (Academic, New York, 1976), Vol. 36.
- <sup>29</sup>S. E. Brown, M. Pieper, W. G. Clark, D. S. Chow, A. Lacerda, and B. Alavi, *J. Phys. IV* **9**, Pr10-187 (1999).
- <sup>30</sup>S. E. Brown, W. G. Clark, and G. Kriza, *Phys. Rev. B* **56**, 5080 (1997).
- <sup>31</sup>W. H. Wong, M. E. Hanson, W. G. Clark, B. Alavi, and G. Grüner, *Phys. Rev. Lett.* **72**, 2640 (1994).
- <sup>32</sup>T. Osada, N. Miura, I. Oguro, and G. Saito, *Phys. Rev. Lett.* **58**, 1563 (1987).